Low-Noise Multispectral Photodetectors Made from All Solution-Processed Inorganic Semiconductors

Jesse R. Manders, Tzung-Han Lai, Yanbin An, Weikai Xu, Jaewoong Lee, Do Young Kim, Gijs Bosman, and Franky So**

Infrared, visible, and multispectral photodetectors are important components for sensing, security and electronics applications. Current fabrication of these devices is based on inorganic materials grown by epitaxial techniques which are not compatible with low-cost large-scale processing. Here, air-stable multispectral solution-processed inorganic double heterostructure photodetectors, using PbS quantum dots (QDs) as the photoactive layer, colloidal ZnO nanoparticles as the electron transport/hole blocking layer (ETL/HBL), and solution-derived NiO as the hole transport/electron blocking layer (HTL/EBL) are reported. The resulting device has low dark current density of 20 nA cm^{-2} with a noise equivalent power (NEP) on the order of tens of picowatts across the detection spectra and a specific detectivity (D^*) value of 1.2×10^{12} cm $Hz^{1/2}$ W^{-1}. These parameters are comparable to commercially available Si, Ge, and InGaAs photodetectors. The devices have a linear dynamic range (LDR) over 65 dB and a bandwidth over 35 kHz, which are sufficient for imaging applications. Finally, these solution-processed inorganic devices have a long storage lifetime in air, even without encapsulation.

1. Introduction

Infrared (IR), visible (vis), and multispectral photodetectors are widely used in optical communications, imaging, security, ranging, and household electronics. Currently, most photodetectors for these applications are grown by epitaxial techniques and after processing the semiconductor dies are then bonded to the read-out integrated circuits. These fabrication processes are costly and usually only allow for small area device fabrication. To mitigate these issues, solution processing of semiconductors is an attractive alternative to significantly lower the fabrication costs, as devices can be processed by large area roll-to-roll processing instead of batch-to-batch wafer processing and are not subject to lattice matching constraints.

J. R. Manders, T.-H. Lai, J. Lee, D. Y. Kim, Prof. F. So
Department of Materials Science and Engineering
University of Florida
Gainesville, FL 32611, USA
E-mail: fso@mse.ufl.edu
Y. An, W. Xu, Prof. G. Bosman
Department of Electrical and Computer Engineering
University of Florida
Gainesville, FL 32611, USA
E-mail: bosman@ece.ufl.edu

DOI: 10.1002/adfm.201402094

Solution-processed devices made from colloidal quantum dots (QDs) are promising for photodetectors operating in the near infrared (NIR), short-wave infrared (SWIR), mid-wave infrared (MWIR) and visible regions.[1,2] QDs are advantageous because their absorption spectrum can easily be tuned by controlling the size of the QDs during synthesis.[3,4] Specifically, lead sulfide (PbS) QDs have been used as the photoactive layer in photodetectors[5–10] due to their tunable absorption across the NIR and visible spectra.

The Sargent group first reported PbS QD photodetectors with a PbS/MEH-PPV polymer blend photoactive layer in a photodiode structure.[11] Subsequently, ligand exchange procedures were used to enhance the charge transport in the QD films, and the resulting photoconductors based on these QD materials had a high responsivity and detectivity.[8] While these photoconductors offer high gains, their speed of response is typically slower than photodiodes due to the presence of traps.[1,7] To address this issue, higher speed Schottky junction photodiodes were fabricated, but these devices yielded lower specific detectivity (D^*) values compared to the slower photodiodes and photoconductors.[10] More recently, the Klimov group fabricated PbS/ZnO and PbS/TiO_2 p-n junction photodiodes that exhibited low noise levels and high detectivity with a high dynamic range.[6] However, the organic carrier transport layers used in the devices are not air-stable.[12,13] Therefore, it is desirable to fabricate high performance all-inorganic PbS QD photodetectors with good air-stability for imaging applications.

In a vertically stacked P-I-N-like photodiode, it is important to have charge-blocking layers inserted between the electrodes and the photoactive layer[14] to reduce the dark current (J_d). While colloidal ZnO nanocrystals have been used as a wide bandgap hole blocking layer/electron transport layer (HBL/ETL) in different optoelectronic devices, most electron blocking/hole transport layers (EBL/HTL) used in solution-processed devices are organic-based transport materials.[14] Previously, we demonstrated that solution-derived NiO is an air-stable wide bandgap p-type semiconductor which can transport holes and block electrons[12] in a polymer solar cell. Thus, we hypothesize that it can function as an EBL/HTL in an all-inorganic double heterojunction photodetector. To fabricate these devices,

the use of both ZnO and NiO wide bandgap semiconductors as carrier blocking layers is expected to reduce the device dark current as well as encapsulate the PbS QD layer. With this device architecture, we demonstrate the first all solution-processed inorganic semiconductor double heterojunction photodetector with a low noise equivalent power (NEP) of tens of picowatts in the visible and infrared working spectra and a high specific detectivity (D^*) value of 1.2×10^{12} Jones (1 cm $Hz^{1/2}$ W^{-1} = 1 Jones). The noise corner frequencies are the lowest reported in the literature for PbS QD-based photodetectors, and the overall noise levels are significantly less than those reported PbS QD-based photoconductors[8] and comparable to the lowest reported PbS QD-based photodiodes.[6,15] The D^* values are similar to those of commercially available Si and InGaAs photodetectors and exceed those of Ge photodetectors. Additionally, due to the presence of the oxides acting as native encapsulation layers, the resulting devices are have a long storage lifetime in air without encapsulation.

2. Results and Discussion

2.1. Device Structure and Materials Properties

In **Figure 1**a, we show the structure of our photodetector with a PbS QD layer sandwiched between a ZnO ETL/HBL and a NiO HTL/EBL to form a double heterojunction. The corresponding band diagram is shown in Figure 1b. Both ZnO and NiO are wide bandgap semiconductors, with ideal band alignment to act as carrier transporting and blocking layers.

PbS QDs were synthesized using the hot injection technique[16] to yield ≈4.5 nm diameter QDs with an absorption edge at approximately 1.3 μm. This synthesis route was previously shown to yield highly air-stable QDs.[16] During device fabrication, a solid-state ligand exchange reaction was carried out to replace the native long insulating oleic acid ligands with shorter 1,3-benzenedithiol ligands. This exchange procedure decreases the spacing between the QDs in the film, and has been shown to increase the QD film conductivity and hence the photoresponse of the photodetectors.[17] Complete fabrication details are provided in the Experimental Section.

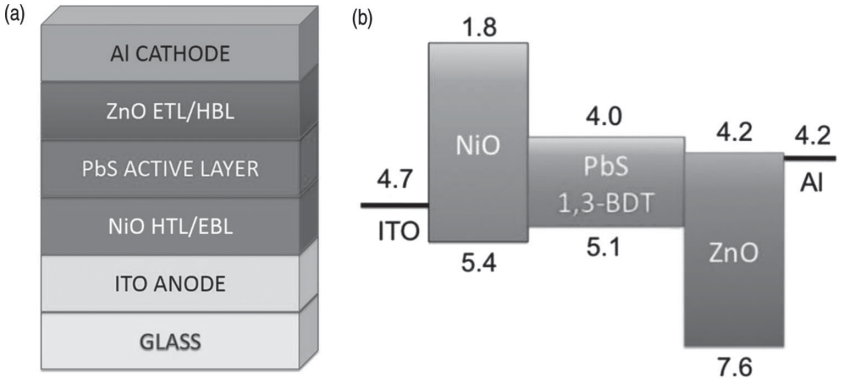

Figure 1. a) The physical device structure for the photodetectors. b) Energy band diagram for the photodetector. The energy band alignments create a double heterojunction structure.

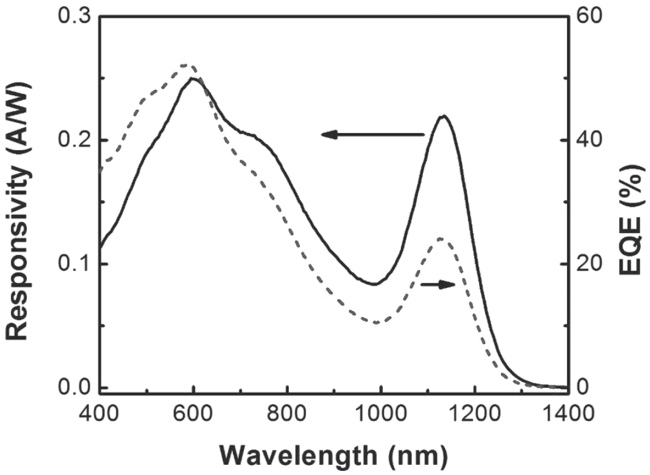

Figure 2. Plot of responsivity and EQE for the photodetectors. EQE in these devices reached 24% at 1130 nm and 52% at 575 nm while the responsivity reached 0.2 A W^{-1} at 1130 nm and 0.25 A W^{-1} at 600 nm. Measurements were taken with a −1 V bias.

2.2. External Quantum Efficiency and Responsivity

The two basic parameters of photodetector sensitivity are the external quantum efficiency (EQE) and the responsivity. **Figure 2** shows the responsivity and EQE at a reverse bias of −1 V. The EQE in these devices reached 24% at 1130 nm and 52% at 575 nm while the responsivity reached 0.2 A W^{-1} at 1130 nm and 0.25 A W^{-1} at 600 nm. These responsivity values are on the same order of magnitude as the values reported for commercially available photodetectors. The broad spectral response of these photodetectors makes them useful for multispectral applications.

2.3. Photodetector Bandwidth

To evaluate these photodetectors for imaging applications, we characterized their temporal response. For typical video applications, a minimum bandwidth of 30 Hz is required. To measure the speed of our devices we used a pulsed light-emitting diode (LED) light source and measured the rise and fall times of the photocurrent on an oscilloscope. In **Figure 3**a, the temporal response data under different bias voltages using a light intensity of 54 mW cm^{-2} at 410 nm are shown. The temporal response of the device is symmetrical with characteristic time constants on the order of a few microseconds. From these data, we calculated the bandwidth from the relation:

$$B = 1/(2\pi\tau) \quad (1)$$

where B is the bandwidth in Hz, and τ is the characteristic time constant of the device. Figure 3b shows the bandwidth as a function of applied bias. The bandwidth of the device increased linearly with applied bias.

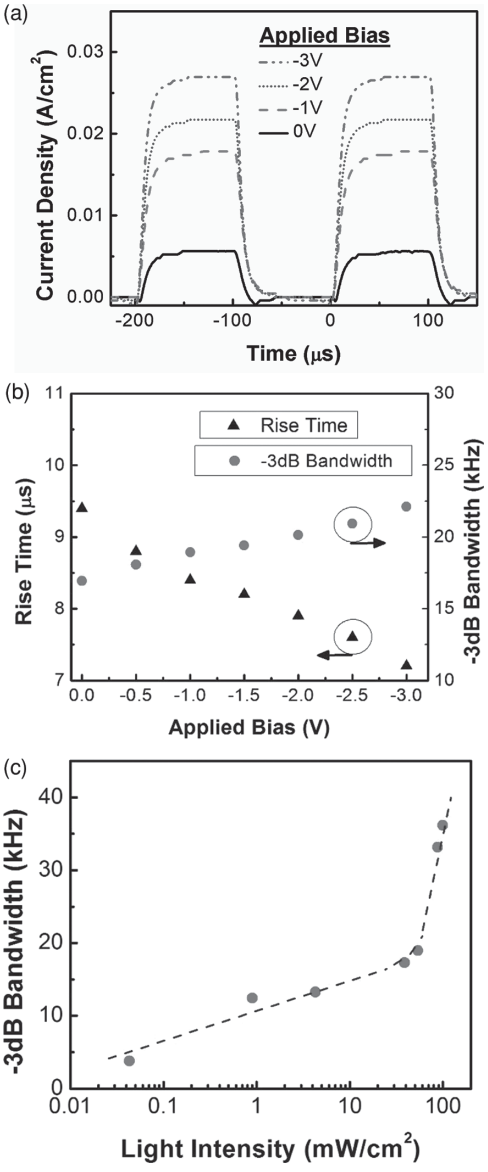

Figure 3. a) Temporal response of the photodetector for light intensity of 54 mW cm^{-2} at 410 nm. b) Speed and bandwidth as a function of applied reverse bias. The bandwidth increases with applied bias. c) Photodetector bandwidth as a function of incident light intensity at −1 V applied bias. As light intensity increases, photoexcited carrier density becomes sufficient to fill traps, allowing an increase in bandwidth.

Additionally, the bandwidth is dependent on the incident light intensity, which indicates that the speed of the photodetector is limited due to the carrier transport in the device stack. The light intensity-dependence of the bandwidth is shown in Figure 3c. Similar light intensity dependence has been shown in other QD-based photodetectors and can be attributed to trap-filling[9,10,15] as explained in the following. Under low intensity excitation, photogenerated carriers are trapped in the QD film, resulting in a slow response. At higher light intensity excitation, a significant portion of the traps are filled by the photoexcited carriers, and the carrier transport becomes trap-free, resulting in a faster photoresponse and a sharp increase in bandwidth. The bandwidth is less than 10 kHz at low intensities and exceeds 36 kHz at high intensities—sufficient for imaging applications. To further ensure the fastest response speed was not limited by RC delay, we measured the capacitance of the photodetector. We found the capacitance to be approximately 1.75 nF and calculated the RC time constant to be approximately 125 ns. The measured capacitance agrees with the theoretical calculation using the layers' dielectric constants and thicknesses. Thus, we conclude the device's response speed is not limited by the RC time constant.

2.4. Noise Characteristics and Detectivity

To further characterize the performance of these photodetectors, it is important to determine the noise characteristics. The noise spectra were measured using a spectrum analyzer, and the data are shown in **Figure 4**a. At high bias voltages, 1/*f* noise was dominant at low frequencies. As the bias voltage was decreased, the DC dark current (J_d) decreased, and the corresponding 1/*f* noise and shot noise decreased. As the 1/*f* noise decreased, the corner frequency (f_c - the transition frequency between the 1/*f* noise and the shot noise) decreased from ≈70 Hz at −3 V to ≈30 Hz at −2.5 V. At biases of −1 V and below, f_c fell below 1 Hz and the entire noise spectrum was dominated by shot noise. The spectrum cutoff for −0.5 V at 10 Hz is caused by the narrow bandwidth on the extremely high gain amplifier setting needed for the low dark current. The f_c values reported here are more than an order of magnitude lower than the lowest previously reported values for PbS QD photodetectors.[5,6] Since this device is a vertically stacked photodiode, and transport is through the bulk, the excess noise contribution from carrier trapping and scattering at surfaces and interfaces, which typically appears in the 1/*f* regime[18,19] in lateral devices such as photoconductors is minimized. Thus, the extremely low corner frequencies are indicative of relatively clean transport through the device since the 1/*f* noise is minimized. The overall low noise levels are generated by low J_d in the device, shown in Figure 4b. The J_d values achieved in the device are 20 nA cm^{-2} at −0.5 V and 34 nA cm^{-2} at −1 V, without any device cooling. It should be noted that the overall noise levels reported here are an order of magnitude lower than those in previously reported PbS QD photoconductors[8] and comparable to the lowest reported values in PbS QD photodiodes.[6,15]

The noise equivalent power (NEP) can be determined from the equation below[6,20,21]

$$NEP = \sqrt{\langle i^2 \rangle}/R \tag{2}$$

where $\langle i^2 \rangle$ is the integrated mean square noise spectral density in the device bandwidth and R is the spectral responsivity. Hence, the specific detectivity, D^*, can be calculated from the equation below:

$$D^* = \frac{\sqrt{A}\sqrt{B}}{NEP} \tag{3}$$

where A is the device area, B is the bandwidth, and NEP is the noise equivalent power.

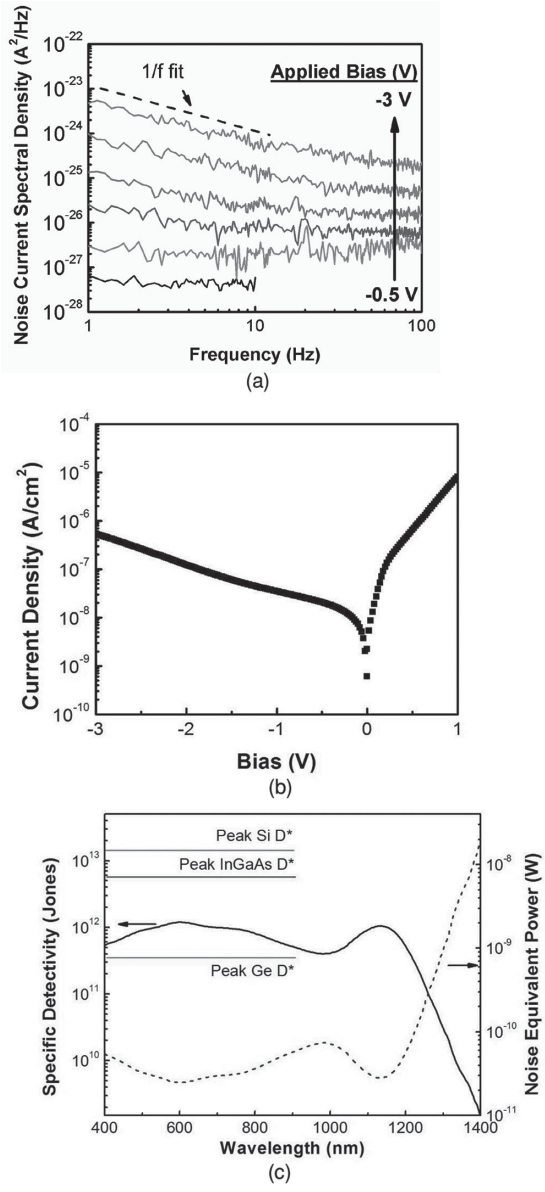

Figure 4. a) Noise current spectral density as a function of frequency and applied bias. The applied bias was changed from –0.5 to –3 V in steps of –0.5 V. At high applied biases, $1/f$ noise appeared with low f_c values. As bias is decreased, J_d decreases and $1/f$ noise is pushed to lower frequencies than measured in our experiment. At –1 V applied bias, the whole bandwidth is shot noise dominated. b) Dark current density vs. applied bias. This plot shows extremely low dark current enabled by the novel double heterostructure. c) Noise equivalent power and specific detectivity of the photodetectors at –1 V. NEP was found to the order of tens of pW across the device's working spectrum. D^* was calculated to be as high as 1.1×10^{12} cm $Hz^{1/2}$ W^{-1} at 1135 nm and 1.2×10^{12} cm $Hz^{1/2}$ W^{-1} at 600 nm. For reference, reported maximum values for D^* in commercial photodetectors are indicated.

Using these relations, we found the NEP at –1 V to be on the order of ten picowatts across the device's working spectrum, as shown in Figure 4c. When the NEP is normalized to a 1 Hz bandwidth standard, it falls to tens of fW $Hz^{-1/2}$. The corresponding peak D^* values are 1.1×10^{12} cm $Hz^{1/2}$ W^{-1} at 1135 nm and 1.2×10^{12} cm $Hz^{1/2}$ W^{-1} at 600 nm. Also shown in Figure 4c are the typical D^* values found in commercially available photodetectors. It is worthwhile to note that the D^* value for our PbS QD photodetector is within an order of magnitude of the detectivity for Si and InGaAs photodetectors and exceeds the D^* value found in Ge photodetectors.

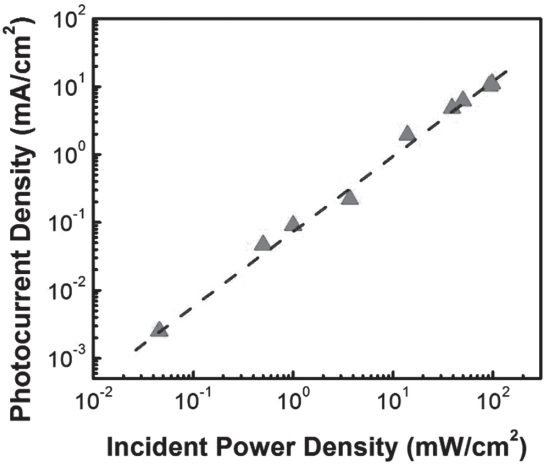

Figure 5. Linear dynamic range (LDR) of the photodetectors measured at –1 V. The total LDR is 67 dB, comparable to InGaAs, and sufficient for high contrast imaging.

2.5. Linear Dynamic Range

Another device parameter important to a photodetector is the linear dynamic range (LDR), which can be calculated using the following equation:

$$LDR(\mathrm{dB}) = 20 \log_{10}(P_{\max} / P_{\min}) \quad (4)$$

where $P_{\max}$ is the highest incident light power and $P_{\min}$ is the lowest incident light power of the range in which the photodetector response is linear with the incident power. **Figure 5** shows the measured LDR of a typical PbS photodetector. The measured LDR extended 67 dB, comparable to the LDR of InGaAs photodetectors.[22]

2.6. Photodetector Stability

Air-stability data for QD-based photodetector devices are not often reported in the literature. However, previous studies on devices using solution processed ZnO and NiO indicate these devices are promising in terms of device lifetime.[12,14] In our previous work, the air-stability of QD photodetectors was significantly improved by the addition of a ZnO HBL/ETL to a control device to protect against oxidative degradation.[14] Additionally, by replacing the traditional PEDOT:PSS HTL/EBL with NiO in polymer solar cells, the devices showed an enhancement in air stability.[12] Thus, we hypothesized that QD photodetectors with both a NiO and a ZnO layer would have a long storage lifetime in air without encapsulation. **Figure 6** shows the stability data over a period of 5 months for a device without

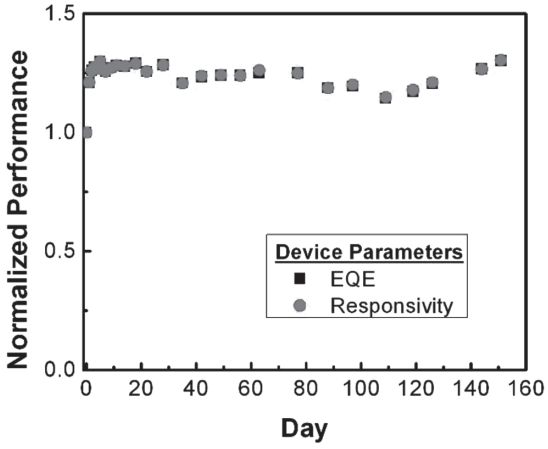

Figure 6. The device's normalized performance through five months of storage in air in the laboratory's ambient conditions without encapsulation.

any encapsulation. During the testing period, the device was stored in the laboratory's ambient environment at room temperature on the measurement bench. In the first few days of storage, the device performance actually improved slightly and subsequently the device remained stable during the entire testing period. The initial improvement in device performance has been reported for other devices with ZnO.[14,23–25] Since colloidal ZnO nanoparticles have a large surface defect density,[26] atmospheric or residual oxygen and moisture can easily bind to their surfaces, thus passivating the film from further reactions with oxygen and moisture. Also, photoexcitation[27] and passivation of the surface defects[28] can enhance the conductivity of ZnO, leading to an improvement in the device performance. Another advantage of using ZnO as an ETL/HBL is that it protects the aluminum cathode from forming an electrically insulating interfacial oxide. Since aluminum cathodes are prone to oxidation, direct contact between the cathode and the photoactive layer or oxidation-prone organic blocking layers causes stability problems.[14] However, when aluminum is in contact with ZnO, as in our photodetectors in this report, any interfacial mixing or oxidation that takes place would not hinder the device performance because aluminum-zinc-oxide is an air-stable n-type transparent conductor.[29] These aging and ZnO interfacial mixing effects have also been observed[25] in a previously reported solution-processed UV photodetector based on a p-n junction of NiO and ZnO. This also led to a long air-storage lifetime. The air stability data suggest that these solution processed PbS QD-based photodetectors are promising for future applications.

3. Conclusion

In summary, we have used PbS QDs as the multispectral absorption sensitizing layer and solution-processed metal oxides for charge blocking layers to fabricate solution-processed all-inorganic multispectral photodetectors. The resulting device has a wide spectral photoresponse from the NIR region through the entire visible spectrum. The bandwidth of these devices is sufficient for imaging applications. The NEP, D^*, and LDR values are comparable to commercially available photodetectors made from expensive vacuum-based epitaxial deposition methods. Finally, with solution-processed air-stable oxides acting as carrier transport and blocking layers, these device are robust with a long storage lifetime.

4. Experimental Section

PbS Synthesis: 0.444g of PbO (Sigma Aldrich) was dissolved with 2 mmol of oleic acid in a three-necked flask under Ar flow with 55 mL of octadecene (ODE). The solution was heated and held at 120 °C. 210 µL of hexmethyldisathiane ($(TMS)_2S$) (Sigma Aldrich) was dissolved in 5 mL of ODE and injected into three necked flasks. The reaction continued for 4 min. The reaction was quenched and precipitated with cold acetone. The QDs were washed and redispersed three times with acetone and chloroform. The final product was stored dry until use.

ZnO Synthesis: The synthesis has been previously published.[27,28] The synthesis was performed by dropwise addition of a stoichiometric amount of tetramethylammonium hydroxide (TMAH) (0.55 M) to 30 mL of 0.1 M zinc acetate dihydrate dissolved in dimethyl sulfoxide (DMSO) under continuous stirring. After precipitation and washing, the nanoparticles were dispersed in pure ethanol.

NiO Precursors: The procedure was previously published for use in solar cells.[12] A 0.1 M solution of nickel acetate tetrahydrate in ethanol was made. A 1:1 mole ratio of monoethanolamine (MEA) to nickel was added as a complexing agent. The solution was stirred until all reagents dissolved into a green solution.

Device Fabrication: The NiO precursor solution was spincast onto solvent-, and UVO_3-cleaned ITO-coated glass substrates and heated to 500 °C in air for one hour to form continuous 15 nm thick NiO films. After cooling, the substrates were transferred to a nitrogen glovebox. PbS layers were spincast from a 5 mg mL^{-1} suspension of QDs in chloroform. After each QD layer deposition, the films were soaked in a 1.0 M solution of 1,3-benzenedithiol in acetonitrile for 1 minute for the ligand exchange. This PbS film deposition and ligand exchange procedure was repeated to yield approximately 250 nm thick QD films. A 20 nm thick layer of ZnO nanoparticles were directly spincast on top and the device was heated to 80 °C for 15 min. Then a 100 nm thick aluminum cathode was thermally evaporated at chamber pressures of $\approx 10^6$ Torr. The final device area was 0.046 cm^2.

Device Characterization: All characterization and noise measurements were performed at room temperature. Current–voltage (*J–V*) characterization was performed with a Keithley 4200 semiconductor parameter analyzer system. EQE and responsivity measurements were conducted using an in-house setup consisting of a xenon DC arc lamp, an ORIEL 74125 monochromator, a Keithley 428 current amplifier, an SR 540 chopper system at 270 Hz and an SR830 DSP lock-in amplifier from SRS. Bandwidth optical measurements were conducted with an in-house pulsed LED setup (Thorlabs). The setup consists of the LED driven by a function generator with a square voltage pulse. The device's current output was amplified by a Stanford SR570 current preamplifier in high bandwidth mode and read by a digital oscilloscope on one channel, while the LED driver was monitored by another channel. Linearity measurements were confirmed by using neutral density filters measured by a Perkin-Elmer UV–Vis spectrophotometer, coupled with broadband solar spectrum light from Newport Thermal Oriel 94021 1000 W solar simulator (4 in. by 4 in. beam size) using the AM1.5 G solar spectrum at 100 mW cm^{-2} incident power. The light intensity was also calibrated by an ORIEL 91150V monosilicon reference cell calibrated by Newport Corporation.

Noise Measurements: Devices were packaged and bonded inside a small aluminum Faraday cage and placed inside a larger solid copper Faraday cage with a SR570 current preamplifier (electrically isolated) which acted as the bias source and amplifier. The solid aluminum and copper boxes shielded the device and amplifier from outside noise. The SR570 amplifier was then connected to an Agilent 35670A Dynamic

Signal Analyzer spectrum analyzer. The spectrum analyzer output the signal directly to the data acquisition setup. A modified setup and equivalent circuit was published previously.[20]

Acknowledgements

The authors thank Alvin Ogden at the University of Florida's Nanoscale Research Facility (NRF) for many fruitful discussions and wirebonding. The authors would also like to thank Erik Klump and Dr. Song Chen of Prof. Franky So's research group for thoughtful insights and helpful discussions. The authors acknowledge the financial support of Nanoholdings LLC.

Received: June 24, 2014
Revised: August 3, 2014
Published online: September 15, 2014

[1] G. Konstantatos, E. H. Sargent, *Nat. Nanotechnol.* **2010**, *5,* 391.
[2] S. Keuleyan, E. Lhuillier, V. Brajuskovic, P. Guyot-Sionnest, *Nat. Photonics* **2011**, *5*, 489.
[3] L. E. Brus, *J. Chem. Phys.* **1983**, *79*, 5566.
[4] L. E. Brus, *J. Chem. Phys.* **1984**, *80*, 4403.
[5] R. Saran, M. N. Nordin, R. J. Curry, *Adv. Funct. Mater.* **2013**, *23*, 4149.
[6] B. N. Pal, I. Robel, A. Mohite, R. Laocharoensuk, D. J. Werder, V. I. Klimov, *Adv. Funct. Mater.* **2012**, *22*, 1741.
[7] G. Konstantatos, E. H. Sargent, *Appl. Phys. Lett.* **2007**, *91*, 173505.
[8] G. Konstantatos, I. Howard, A. Fischer, S. Hoogland, J. Clifford, E. Klem, L. Levina, E. H. Sargent, *Nature* **2006**, *442*, 180.
[9] G. Konstantatos, J. Clifford, L. Levina, E. H. Sargent, *Nat. Photonics* **2007**, *1*, 531.
[10] J. P. Clifford, G. Konstantatos, K. W. Johnston, S. Hoogland, L. Levina, E. H. Sargent, *Nat. Nanotechnol.* **2009**, *4*, 40.
[11] S. A. McDonald, P. W. Cyr, L. Levina, E. H. Sargent, *Appl. Phys. Lett.* **2004**, *85*, 2089.
[12] J. R. Manders, S.-W. Tsang, M. J. Hartel, T.-H. Lai, S. Chen, C. M. Amb, J. R. Reynolds, F. So, *Adv. Funct. Mater.* **2013**, *23*, 2993.
[13] M. Jørgensen, K. Norrman, F. C. Krebs, *Sol. Energy Mater. Sol. Cells* **2008**, *92*, 686.
[14] G. Sarasqueta, K. R. Choudhury, J. Subbiah, F. So, *Adv. Funct. Mater.* **2011**, *21*, 167.
[15] T. P. Osedach, N. Zhao, S. M. Geyer, L.-Y. Chang, D. D. Wanger, A. C. Arango, M. C. Bawendi, V. Bulović, *Adv. Mater.* **2010**, *22*, 5250.
[16] H. Fu, S.-W. Tsang, Y. Zhang, J. Ouyang, J. Lu, K. Yu, Y. Tao, *Chem. Mater.* **2011**, *23*, 1805.
[17] G. Sarasqueta, K. R. Choudhury, F. So, *Chem. Mater.* **2010**, *22*, 3496.
[18] M. J. Kirton, M. J. Uren, *Adv. Phys.* **1989**, *38*, 367
[19] F. N. Hooge, *IEEE Trans. Electron Devices* **1994**, *41*, 1926.
[20] Y. An, H. Rao, G. Bosman, A. Ural, *J. Vac. Sci. Technol. B* **2012**, *30*, 021805.
[21] G. Konstantatos, E. H. Sargent, *Proc. IEEE* **2009**, *97*, 1666.
[22] X. Gong, M. Tong, Y. Xia, W. Cai, J. S. Moon, Y. Cao, G. Yu, C.-L. Shieh, B. Nilsson, A. J. Heeger, *Science* **2009**, *325*, 1665.
[23] D. Bi, G. Boschloo, S. Schwarzmüller, L. Yang, E. M. J. Johansson, A. Hagfeldt, *Nanoscale* **2013**, *5*, 11686
[24] H. Wang, T. Kubo, J. Nakazaki, T. Kinoshita, H. Segawa, *J. Phys. Chem. Lett* **2013**, *4*, 2455.
[25] D. Y. Kim, J. Ryu, J. Manders, J. Lee, F. So, *ACS Appl. Mater. Interfaces* **2014**, *6*, 1370.
[26] S. Chen, J. R. Manders, S.-W. Tsang, F. So, *J. Mater. Chem.* **2012**, *22*, 24202.
[27] S. Chen, C. E. Small, C. M. Amb, J. Subbiah, T.-H. Lai, S.-W. Tsang, J. R. Manders, J. R. Reynolds, F. So, *Adv. Energy Mater.* **2012**, *2*, 1333.
[28] M. Hartel, S. Chen, B. Swerdlow, H.-Y. Hsu, J. Manders, K. Schanze, F. So, *ACS Appl. Mater. Interfaces* **2013**, *5*, 7215.
[29] J. Hu, R. G. Gordon, *J. Appl. Phys.* **1992**, *71*, 880.